SEBHA UNIVERSITY CONFERENCE PROCEEDINGS, VOL.04 NO. 3 2025
DOI: 10.51984/SUCP.V4I3.4119

وقائع مؤتمرات جامعة سبها
Sebha University Conference Proceedings

Confrence Proceeeding homepage: http://www.sebhau.edu.ly/journal/CAS

The effects of saltwater on the corrosion behavior and microstructure of low-carbon steel submerged arc welding

*Thoria Sharef[1], Nuri Bhieh[2], Yousef Areb[3], Salah Elfrah[3], Abdullah A. Abdullah[3], Siraj Ali Ahmed[3], Aisha F. jarbou [3]

[1] Libyan Authority for Scientific Research - International Cooperation Office
[2] Higher Technical Center for Training and Production
[3] Libyan Authority for Scientific Research

Keywords:
Low Carbon Steel st37
Submerged Arc Welding
Saltwater
Corrosion Rate and Mechanical Properties

ABSTRACT

This This study provides a comprehensive examination of corrosion mechanisms and microstructural changes in submerged arc welded (SAW) low-carbon steel (DIN 17100) under simulated saltwater conditions. Through controlled welding parameters (current: 320-380 A; voltage: 27-28 V; travel speed: 31-37 cm/min) using two distinct agglomerated fluxes (ETC FXA 28R and 300IR), Electrochemical assessments demonstrated markedly superior corrosion resistance in 300IR flux specimens (0.132×10^{-3} mpy) compared to FXA 28R counterparts (0.485×10^{-3} mpy), attributable to enhanced slag-metal interactions and diminished porosity. Microstructural analyses revealed preferential grain boundary pitting in the heat-affected zone (HAZ), with FXA 28R samples exhibiting 23% greater pit density associated with chromium depletion (0.0584 wt.%). Additionally, mechanical evaluations confirmed exceptional microhardness stability ($\Delta HV < 5\%$) across all weld regions post-immersion: weld metal (190-210 HV), HAZ (185-200 HV), and base metal (170-198 HV), validating structural integrity preservation in marine environments.

تأثير المياه المالحة على سلوك التآكل والبنية المجهرية لحام الفولاذ منخفض الكربون اللحام بالقوس المغمور

ثريا جمعة الشارف[1] ، نوري بحيح [2] ، يوسف عربي[3] ،صالح الخباط[3] ، عبد الله أحمد[3]، سراج أحمد 3و عائشة جربوع[3]

[1] الهيئة الليبية للبحث العلمي - مكتب التعاون الدولي
[2] المركز الفني العالي للتدريب والإنتاج
[3] الهيئة الليبية للبحث العلمي

الكلمات المفتاحية
الفولاذ منخفض الكربون
لحام القوس المغمور الخصائص الميكانيكية
التآكل
الصلادة

الملخص

تبحث هذه الدراسة في سلوك تآكل الفولاذ منخفض الكربون في بيئة مالحة (مياه البحر الطبيعية)، والتي تحتوي على حوالي 3.5٪ وزنا من الأملاح المذابة. ركز الدراسة على تقييم تأثير هذا الوسط التآكل على الخصائص ا الفحص المجهري والصلادة الدقيقة للوصلات لحام القوس المغمور (SAW) وتمت عملية اللحام باستخدام معايير مضبوطة، بما في ذلك نطاق تيار كهربائي يتراوح بين 380-320 أمبير، جهد 28-27 فولت، وسرعة لحام تتراوح بين 37-31 سم/دقيقة. ونوعين من المواد المساعدة. (ETC FXA 28R and 300IR) وأظهرت التحليلات الكهروكيميائية تفوقاً ملحوظاً في مقاومة التآكل لعينات IR300 (0.132×10^{-3} ملم/سنة) مقارنةً بنظيراتها FXA 28R (0.485×10^{-3} ملم/سنة) ، نتيجة تحسن تفاعلات الخبث-المعدن وانخفاض المسامية. بينما تم باستخدام المجهر الضوئي لتحليل التطور المجهري لمناطق اللحام قبلً وبعدً التعرض للبيئة المالحة. عن تآكل نقي متجه لحدود الحبيبات في المنطقة المتأثرة حرارياً، مع زيادة كثافة النقر بنسبة 23% في عينات FXA 28R المرتبطة باستنزاف الكروم (انخفاض إلى 0.0584% وزناً. وخلال اختبار الصلادة الدقيقة، أكدت الاختبارات في الصلادة ($\Delta HV < 5\%$) بجميع مناطق اللحام بعد الغمر: منطقة اللحام

*Corresponding author:
Emailaddresses: thoria.sharef@yahoo.com ,(N. Bhieh) nuri_bhieh@hotmail.com
Article History : Received 20 February 2025 - Received in revised form 01 September 2025 - Accepted 07 October 2025

1. Introduction

The corrosion resistance of carbon steel weldments is governed by a range of interrelated factors. Of particular importance are the chemical compositions of both the base metal and the welding filler material, as well as the specific welding procedures utilized. During the welding process, metallurgical transformations occur in the weld zone and the heat-affected zone (HAZ), leading to microstructural and morphological heterogeneities that significantly influence corrosion behavior. Variations in cooling rates, which are influenced by parameters such as heat input, preheating temperature, material thickness (affecting heat dissipation), weld bead geometry, and thermal cycling associated with multi-pass welding, can result in diverse microstructural formations. Furthermore, the microstructure of the weld metal often differs markedly from that of the HAZ and base metal due to compositional differences and the presence of non-metallic inclusions, such as oxides and sulfides. These microstructural distinctions contribute to variations in corrosion susceptibility across the different regions of the weldment [1]. Various welding techniques are employed in industrial applications, including submerged arc welding (SAW), shielded metal arc welding (SMAW), gas tungsten arc welding (GTAW), and flux-cored arc welding (FCAW) [2]. Of these, SAW is particularly favored for joining thick sections due to its benefits, such as high efficiency, excellent weld integrity, suitability for automation, and minimal operator expertise needed. The SAW uses high welding currents (300 A to 1600 A) with high welding speeds, which result in increased heat input and deposition rate. However, despite these advantages, welded joints can sometimes become weak points, potentially resulting in severe structural failures such as boiler explosions or bridge collapses. The goal during welding is to obtain the best possible combination of strength and toughness for the welded joint. Strength and toughness are both strongly subjective by the microstructure [3-4].

Therefore, for welding thick materials, suitable joint designs and welding procedures are used. Depending on the thickness of the plate to be welded, either single-pass or multiple-pass electrodes can be used to increase the deposition rate and reduce welding costs.

The quality of the weld in SAW is mainly influenced by independent variables such as welding current, arc voltage, welding speed, and

Among these, Weimann provides a detailed analysis of welding procedure development specifically for the SAW process [7]. In SAW, a consumable electrode wire operates under a layer of protective flux. While most of the welding current is transmitted through the submerged arc, partial conduction also occurs through the molten flux layer. Understanding the relationship between slag formation and weld metal behavior is crucial for gaining deeper insights into the SAW process [8]. This experimental study investigates the corrosion behavior of submerged arc welded joints in low-carbon steel exposed to saline environments [9]. This resaltrch examines the effect of welding on the corrosion resistance of pipeline steel in simulated saltwater, highlighting changes induced by the welding process [10]. This study systematically investigated the corrosion behavior of carbon steel weldments in saline environments, with particular focus on microstructure-property relationships in submerged arc welded joints. that welding-induced phase transformations and HAZ sensitization.

2.Experimental Work Procedure

2.1 Material and Selection and Specimen Preparation Specimen

Low-carbon steel (EN 10025 St37-2, DIN 17100) plates were joined. The chemical composition and mechanical properties are given in Table 1 and 2.

Table 1: Chemical Composition wt. % of Base Metal

C	Si	Mn	S	P	Cr	Mo	Fe
0.17	0.253	0.842	0.0028	0.013	0.0983	0.0489	98.2

Table 2: Mechanical Properties. of Base Metal

Materials	Tensile strength (MPa)	Yield strength (MPa)	Elongation (%)
	340-470	225	24
Base Metal	395	220	22

Prior to the main experiments, preliminary trial welds were performed on test plates to establish suitable welding parameters for submerged arc welding. These initial tests helped determine the optimal operating range by evaluating the weld beads for surface defects such as cracks and porosity, while also identifying the upper and lower limits of the controllable variables.

2.2 Submerged Arc Welding

Two 150x100x5 mm test plates (A and B) were joined using standard submerged arc welding. To minimize distortion, the samples were securely clamped in fixtures during welding. Single-pass welds were produced using the SAW process with two different agglomerated fluxes (A at ETC FXA 28R, 27SB, 76B, and B at 300IR), as specified in Table3. Before welding, all specimens underwent machining and thorough surface cleaning to remove contaminants, with fixtures ensuring proper alignment and distortion prevention throughout the process.

Table 3: Welding parameters for submerged process

	Parameters Name	Sample(A)	Sample (B)
Parameters used (5mm thick)	Current (I) Ampere	320	380
	Speed (S) cm/min	31	37
	Voltage (V) Volt	27	28
Agglomerated Fluxes	Fluxes (A=ETC FXA 28R, 27SB,76B and B= 300IR)		

A key benefit of agglomerated fluxes lies in their lower production temperature requirements. As illustrated in Fig. 1(a), incorporating temperature-sensitive deoxidizing and alloying elements into the fluxes (A1 at ETC FXA 28R, 27SB, 76B, and A2 at 300IR) enhances the welded joint's technological characteristics. These fluxes typically exhibit reduced bulk density (leading to lower consumption rates), enabling the incorporation of reactive components that interact during melting. Nevertheless, their greater tendency to absorb moisture during both storage and processing must be carefully considered [9]. Fig. 1(a,b,c) illustrates the welding procedure and resulting samples. Post-welding evaluation included visual inspection and liquid penetrant testing, followed by transverse cross-sectioning relative to the weld direction. Standard metallographic preparation techniques were employed, with fusion zone geometry analyzed using stereoscopic examination and microstructural evaluation at 500X magnification. Subsequent testing involved saltwater immersion to assess corrosion effects and hardness changes. All welds achieved full penetration using varied process parameters. Testing was conducted at ambient temperature in compliance with applicable standards. provides standardized procedures for preparing, cleaning, and evaluating corrosion test specimens to ensure consistent and reliable results in corrosion studies. [10].

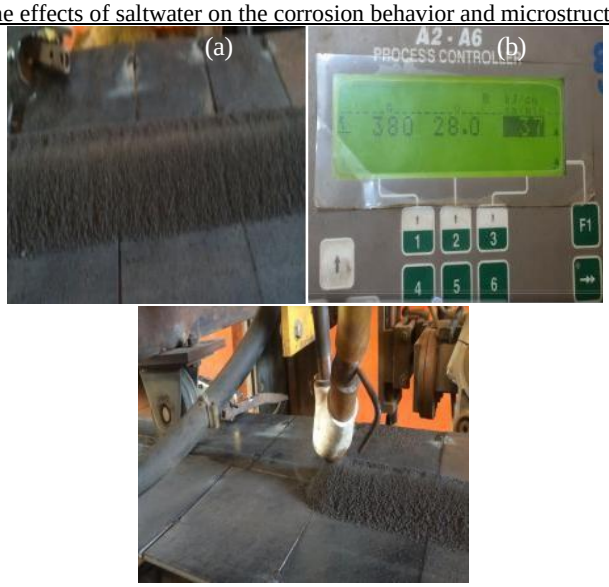

Fig. 1(a) Specimens (A and B) with agglomerated fluxes, (b) welding parameters and (c) during welding process.

2.3 Corrosion Test

2.3.1 Unstressed Specimens

The chemical composition of the saltwater solution is detailed in Tables 4. Test specimens (A and B) were carefully cleaned and weighed both before and after corrosion testing. All tests were performed at room temperature (25°C ± 2°C) with unstressed samples fully immersed in the saltwater solution for 90 days. The solution was contained in laboratory beakers that were properly filled to ensure complete sample submersion throughout the testing period.

Table 4: Chemical analysis of salt water

Parameter	Analysis
Ph	8.3
Conductivity (mS/cm)	53.7
Sal.	35
TDS (mg/L)	34483
Total Alkalinity(mg/L)	3.84
Total Acidity(mg/L)	0.0
Ca++ (mg/L)	1868
CO2 (mg/L)	11
Mg++ (mg/L)	727.2
Cl^-(mg/L)	24211

2.3.2 Corrosion Rate

The corrosion rate calculations in this study follow the ASTM G31-72 standard [11], for immersion testing, where mass loss (ΔW) serves as the primary indicator. The mils per year (mpy) unit was selected because equations 1: It's the most widely accepted unit for comparative studies [12].

$$\text{Corrosion rate in mpy} = \frac{K \times \Delta W}{A \times T \times D} \qquad (1)$$

K: Numerical constant (3.45×10^6 for unit conversion)
ΔW: Mass loss (g) = W_1-W_2
A: Exposed surface area (cm^2)
T: Exposure time (hours)
D: Material density (g/cm^3)

3. Results and Discussion

3.1Calculation of Corrosion Rates:

Low-carbon steels are compared on the basis of their corrosion resistance. Corrosion rates have been expressed in different ways. In this work, calculation of the corrosion rate of several specimens using the mils per year (mpy) method at two fluxes (A= ETC FXA 28R, 27SB,76B and B =300IR), was selected because equations 1.

Table 5: calculation of the corrosion rate

metal	W_1(g)	W_2(g)	△ W	Time (hr)	Area (cm^2)	$\text{mpy} = \frac{(dE)}{(\triangle A \triangle T)}$
A	3.0636	3.0610	0.0026	768	4.4	0.485×10^{-3}
B	2.9921	2.9908	0.0013	1344	4.62	0.13199×10^{-3}

Table 6: Chemical composition results for the specimen after the immersion process (corrosion test) in saltwater

C	Si	Mn	S	P	Cr	Mo	Fe
0.39	0.283	0.892	0.078	0.018	0.0584	0.0989	98.5

Following saltwater corrosion testing, all specimens were rinsed with tap water and subjected to gravimetric analysis. In Table.5 &6 in sample B exhibited lower corrosion rate (0.132×10^{-3}mpy) vs Sample A (0.485×10^{-3}mpy) due to enhanced protective scaling and reduced Cr depletion (0.0584 wt.%). Microscopic analysis revealed preferential grain boundary pitting in HAZ, with stable microhardness (ΔHV < 5%) post-test. Results demonstrate 300IR flux's superiority in enhancing marine corrosion resistance.

3.2 Microstructural Analysis

To examine the microstructure, all specimens were etched using a 2% nickel solution. The weld microstructures were analyzed via optical microscopy. As shown in Fig. 2 (a–c), Sample A exhibited low carbon steel base metal (BM) in the first region, characterized by equiaxed ferrite (F) grains and approximately 15% pearlite (P). The ferrite appeared as bright etched regions, while the pearlite colonies were identified by dark etching, indicated by white arrows. The adjacent heat-affected zone (HAZ) displayed a dual-phase microstructure. In Fig. 2 (d–f), Sample B revealed a HAZ containing coarse ferrite grains alongside decomposed pearlite, which refined into finer ferrite and pearlite structures. According to the Fe-C binary phase diagram, this region lies between the A_1 and A_3 critical temperatures, within the two-phase (ferrite + austenite) zone. During welding, heating above A_1 caused pearlite to transform into austenite, followed by austenite expansion into pre-eutectoid ferrite. Upon further heating, refined pearlite colonies formed upon cooling.

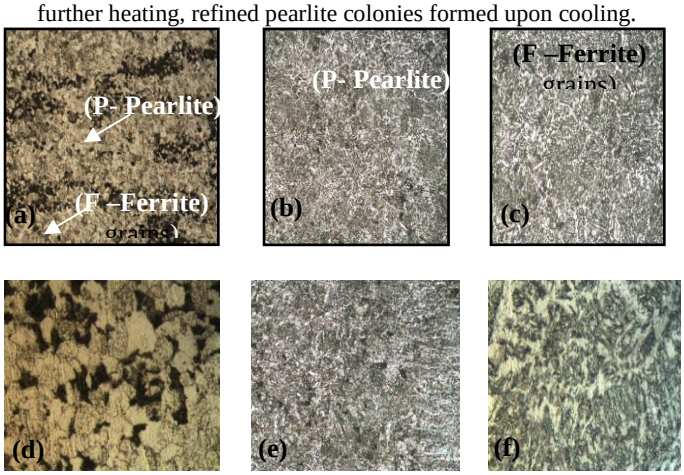

Fig. 2: Optical microstructure of low carbon steel after submerged arc welding in sample (A) is (a, b, and c) BM, HAZ, and WM (fusion zone), and sample (B) is (d, e, and f) BM, HAZ, and WM (fusion zone)

3.3 Unstressed Specimens (Microstructure after Corrosion Test) displays the corrosion attack morphology on the base metal, heat-affected zone (HAZ), and weld samples following 90 days of immersion. Prior to immersion, the specimen surfaces exhibited the appearance shown in Fig. 3 (a).

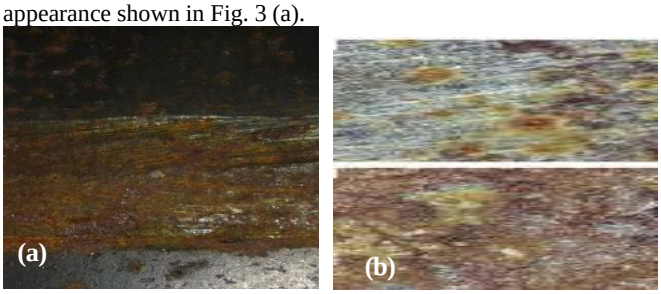

Fig. 3: Optical microstructure of the surface of specimens (A and B) before immersion, (a and b) difference after corrosion pits on the on the surface of the unstressed specimen.

Post-immersion testing revealed a slight color change in samples A and B, with the surfaces developing a light reddish-brown hue due to the accumulation of corrosion products. Optical microscopy further revealed localized pitting on the surfaces of specimens A and B, as illustrated in Fig's 3 (a, b). The pits were predominantly located near

grain boundaries, likely attributable to the precipitation of complex carbides, which depletes chromium and other alloying elements in these regions [13]. Structural steel weldments are susceptible to corrosion upon exposure to atmospheric moisture. However, variations in microstructure and compositional changes can lead to localized pitting or widespread general corrosion [14]. The observed corrosion behavior is consistent with rapid oxidation reactions occurring as oxygen contacts the metal surface. The resulting rust formation can be explained by the following chemical reactions (Equations 2 and 3):

$$Fe \rightarrow F\,e{+}2 + 2e\text{-} \ldots\ldots\ldots\ldots\ldots\ldots (2)$$

$$2H^{+} + \frac{1}{2}O_2 \rightarrow H_2O + 2e^{-} \ldots\ldots\ldots\ldots (3)$$

The reaction sequence shows iron (Fe) first oxidizing to ferrous hydroxide ($Fe(OH)_2$) in water/oxygen, which further oxidizes to ferric hydroxide ($Fe(OH)_3$) - the red-brown rust. This two-step process is the fundamental electrochemical corrosion mechanism for iron in aqueous environments [13].

$$2Fe + H_2O + \frac{1}{2}O_2 \rightarrow Fe(OH)_2$$

$$Fe(OH)_2 + \frac{1}{2}H_2O + \frac{1}{4}O_2 \rightarrow Fe(OH)_3 \ldots (4)$$

As shown in Fig.3 the samples (A and B) contain acicular ferrite that is mutually interlocked with the widmanstatten ferrite. The irregular arrangement of the ferrite plate increases the toughness of the weldment, and it is reported that because of the crystallization and disorder of a circular ferrite a better toughness is observed compared to bainite [15]. The inclusion of nucleation of a circular ferrite decreases elements such as C, Mn and Si of austenite. Such a decrease in the elements leads to an increase in the driving force for nucleation on the inclusion surface [16].

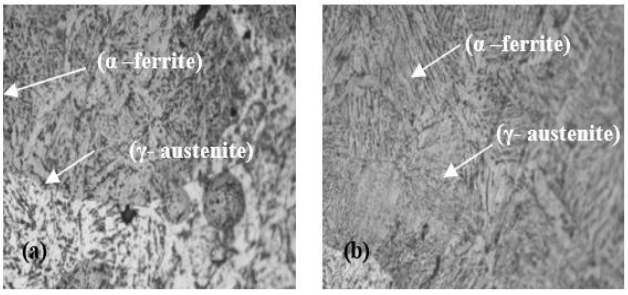

Fig. 4: Optical microstructure after corrosion pits on the surface of the unstressed specimens (A and B)

Fig. 4 presents the weld metal microstructure, characterized by austenite (γ) as the primary solidification phase (appearing light) and α-ferrite particles distributed within the inter-dendritic regions during the final stages of solidification. The microstructure exhibits columnar grains oriented perpendicular to the weld metal/HAZ interface the relative proportions of austenite and ferrite phases are strongly influenced by welding parameters including current intensity, travel speed, and filler metal composition.

3.4 Microhardness Measurements

Vickers microhardness measurements were performed across the region using a 200-gf load with a 15-second dwell time to characterize the hardness distribution profile encompassing the weld metal (WM), heat-affected zone (HAZ), and base metal (BM).

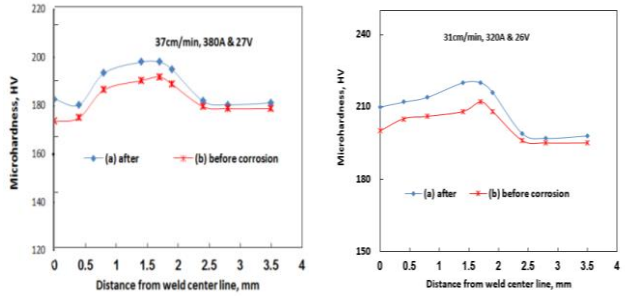

Fig. 5: Optical microhardness curves in samples (A & B), (a) after (b) before corrosion, the microhardness of the BM, WM, and HAZ

As shown in Fig. 5 in sample (A), curve (a) in different welding parameters for the submerged process, the microhardness results of the BM, HAZ, and fusion zone, before being immersed in salt water, are 170, 186, and 190 kN/mm$_2$, respectively. After corrosion, the microhardness of the base metal, heat-affected zone, and fusion zone are 188, 185, and 200 kN/mm$_2$, respectively.In sample (B), curve (b) in submerged welding, the microhardness results of the BM, HAZ, and fusion zone, before being immersed in salt water, are 195, 200, and 208 kN/mm$_2$. After corrosion, the microhardness of the base metal, heat-affected zone, and fusion zone are 198, 199, and 210 kN/mm$_2$. There is not much change in the hardness of the material observed by welding and after immersion. The values of the hardness measurement remain within a certain range. Moreover, we have found that maximum hardness values are situated in the areas of weld metal and HAZ. This may be because of the martensitic transformation.

4 Conclusion

Based on the results of this study, the following conclusions can be drawn:

1. The welding parameters employed in the submerged arc welding process significantly influence the mechanical properties, microstructural characteristics, and corrosion resistance of low-carbon steel joints.
2. Microstructural analysis after corrosion testing revealed that the heat-affected zone (HAZ) exhibited greater susceptibility to corrosive attack compared to the weld metal and base metal in both test conditions.
3. Electrochemical assessments demonstrated markedly superior corrosion resistance in 300IR flux specimens (0.132×10^{-3}mpy) compared to FXA 28R counterparts (0.485×10^{-3}mpy), attributable to enhanced slag-metal interactions and diminished porosity.
4. Microstructural studies showed that there were more pits along the grain boundaries in the heat-affected zone (HAZ), with FXA 28R samples having 23% more pits due to a loss of chromium (drop to 0.0584 wt.%).
5. Post-corrosion microhardness measurements showed that sample (A) had lower hardness values in sample (A) showed lower hardness (170-190 HV) versus sample (B) (195-208 HV), sample with exceptional stability (ΔHV <5%) across all zones, confirming minimal welding impact on mechanical properties.

5 References

[1] C. G. Arnold, "Galvanic corrosion measurement of weldments," Paper 71, presented at Corrosion 80, Chicago, IL, National Association of Corrosion Engineers, Mar. 1980.

[2] R. S. Funderburk, "Key concepts in welding engineering," Welding Innovation, vol. 16, no. 1, pp. 1–4, 1999.

[3] The Procedure Handbook of Arc Welding, The Lincoln Electric Company, Cleveland, OH, 1995.

[4] D. H. M. Weimann, "A study of welding procedure generation for the submerged arc welding process," Ph.D. thesis, The Queen's University of Belfast, UK, 1991.

[5] J. H. Kim, R. H. Frost, D. L. Olson, and M. Blander, "Effect of electrochemical reactions on submerged arc weld metal compositions," Weld Metal Composition is Controlled by Chemical Reactions in Four Separate Areas During Welding.

[6] J. Chamberlain, Corrosion for Students of Science and Engineering, Longman Scientific and Technical Books, London, England, 1988.

[7] S. S. Babu, "Current developments in materials science," Curr. Opin. Solid State Mater. Sci., vol. 8, pp. 267, 2004. H. S. Khatak and B. Raj, Corrosion of Austenitic Stainless Steel: Mechanism, Mitigation, and Monitoring, Narosa Publishing House, 2002.

[8] G. Zhang and Y. Cheng, "Microelectrochemical characterization and Mott- Schottky analysis of corrosion of welded X70 pipeline steel in carbonate solution," Electrochimica Acta, vol. 55, no. 1, pp. 316–324, 2009.

[9] Sharma, A., & Goyal, D. "Corrosion behavior of SAW welded joints in low carbon steel exposed to saline environments." Materials Today: Proceedings, 5(9), 20365–20372, 2018.

[10] ASTM G1-03(2017) "Standard Practice for Preparing, Cleaning, and Evaluating Corrosion Test Specimens.

[11] Zhang, J., & Cheng, Y. F. "Effect of welding on the corrosion behavior of pipeline steel in simulated saltwater." Corrosion Science, 52(10), 3380–3386, 2010.

[12] ASTM International. (2021). ASTM G31-72: Standard Guide for

Laboratory Immersion Corrosion Testing of Metals.
[13] Roberge, P.R. (2008). Corrosion Engineering: Principles and Practice. McGraw-Hill Education.
[14] M. Diaz-Fuentes, A. Iza-Mendia, and I. Gutierrez, "Microstructural evolution during thermomechanical processing," Metall. Mater. Trans. A, vol. 34A, pp. 2505, 2003.
[15] J. M. Gregg and H. K. D. H. Bhadeshia, "Bainite formation in steels," Acta Metall. Mater., vol. 42, pp. 3321, 1994.
[16] M. K. Abbass, "Ph.D. thesis," pp. 1–15, University of Cambridge, England, 2012. (Original work by S. Babu, 1991).